Supporting Information

Water inhibition of oxymethylene dimethyl ether synthesis over zeolite H-Beta: a combined kinetic and *in situ* ATR-IR study

Christophe J. Baranowski [a †], Thibault Fovanna [a, b †], Maneka Roger [a, b], Matteo Signorile [c], Joseph McCaig [a], Ali M. Bahmanpour [a], Davide Ferri [b], Oliver Kröcher [a, b*]

[a] *Institute of Chemical Sciences and Engineering, École Polytechnique Fédérale de Lausanne (EPFL), 1015 Lausanne, Switzerland*

[b] *Paul Scherrer Institut, Forschungstrasse 111, 5232 Villigen PSI, Switzerland.*

[c] *Department of Chemistry, NIS Centre and INSTM Reference Center, University of Turin, via P. Giuria 7, 10125 Turin, Italy*

[†] *These authors contributed equally to the publication*

** Corresponding author: oliver.kroecher@psi.ch; Tel: +41 (0)56 310 20 66*

1. Equilibrium constant calculation

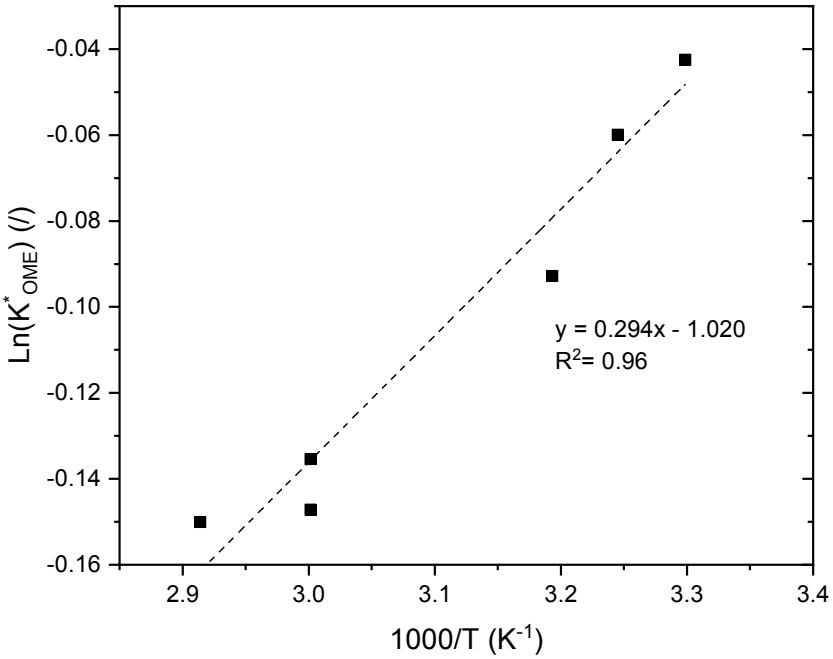

Fig. S1. Van't Hoff plot of the experimental values of K^*_{OME}. The model is indicated by a dashed line. The OME synthesis process was performed with an OME_1/TRI ratio of 3.3 and 0.5 wt % of catalyst.

2. DFT simulations

2.1. Models

DFT calculation aimed at supporting experimental evidences from both the kinetic and the ATR-IR study. The relative stability of the two most stable isomers of both OME_1 and TRI was evaluated. The structure of the adopted molecular models is reported in Fig. S2.

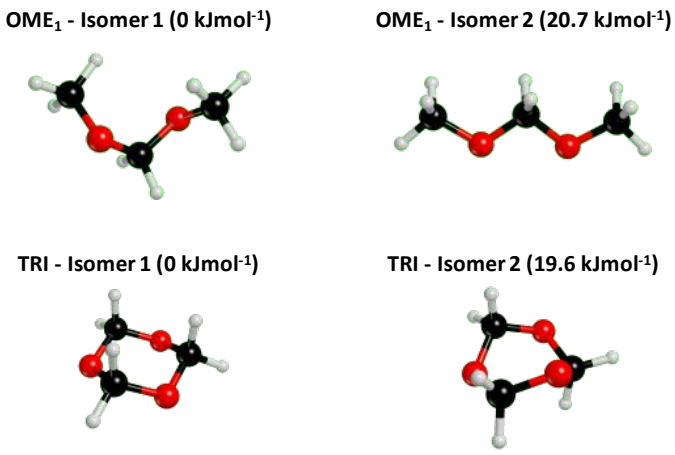

Fig. S2. Molecular models of the most stable isomers of OME_1 and TRI adopted in the B3LYP-D3/CBS simulations. The relative stability (ΔG) of the isomers for of each molecule is reported in brackets.

We further simulated the interaction of OME_1, TRI and water with a minimal BAS model and the optimized adduct structures are shown in Fig. S3. We report here only the results concerning the adsorbates of the most stable isomers of both OME_1 and TRI over BAS, since adsorption does not alter significantly the relative stability of the isomers.

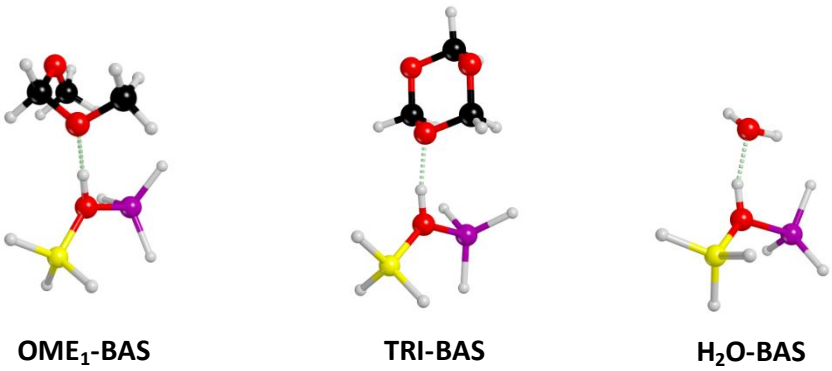

Fig. S3. Molecular models of the OME_1, TRI and H_2O adsorbates with BAS, as adopted in the B3LYP-D3/CBS simulations. Colors: H (white), C (black), O (red), Al (pink) and Si (yellow).

2.2. Complete basis set (CBS) extrapolation

In order to compute accurate electronic energies, a CBS extrapolation strategy was adopted. We performed single point calculations at the B3LYP-D3/6-31+G(d,p) relaxed geometry by exploiting the same Hamiltonian, but adopting the Dunning aug-cc-pVnZ (with n = 2,3,4, here indicating the maximum angular momentum L of functions included in the basis) basis sets. The B3LYP/CBS electronic energies were obtained by linear extrapolation at n = 0 for the single point energies vs n^{-3}, as exemplified for OME_1 (Isomer 1) in Fig. S4.

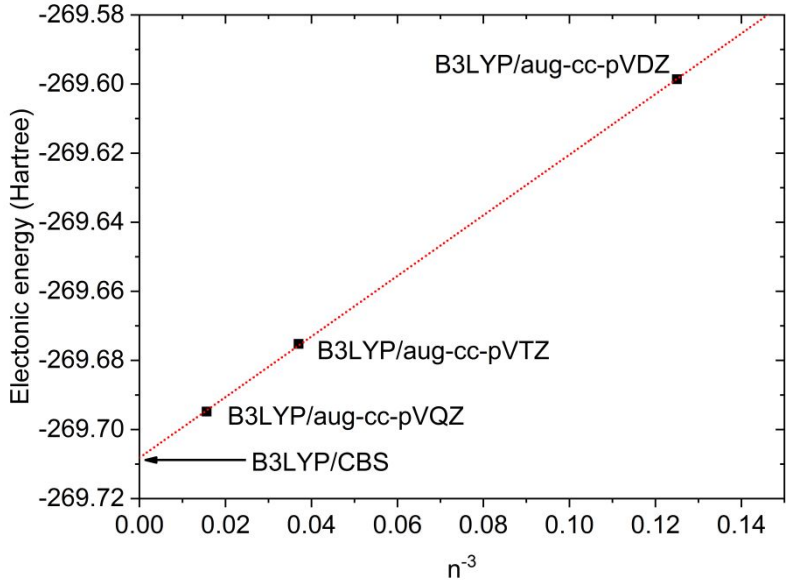

Fig. S4. CBS extrapolation for OME_1 (Isomer 1).

3. Catalyst characterization

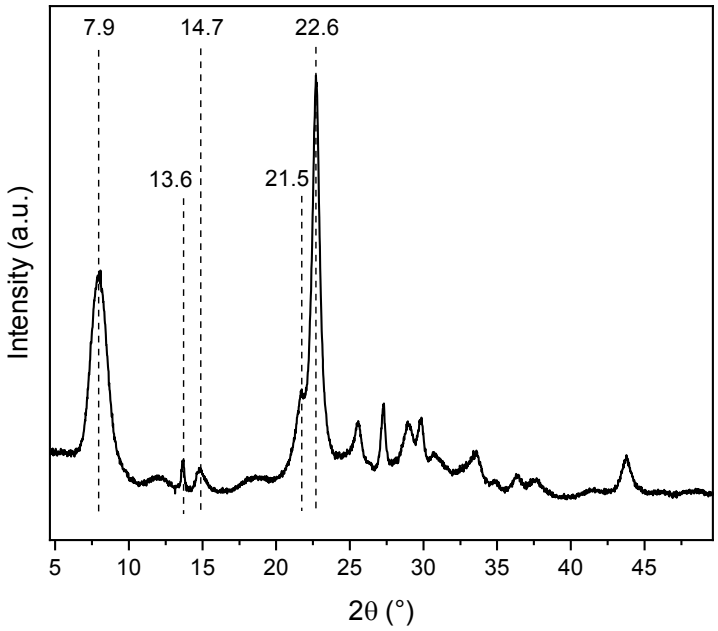

Fig. S5. XRD pattern of zeolite H-Beta.

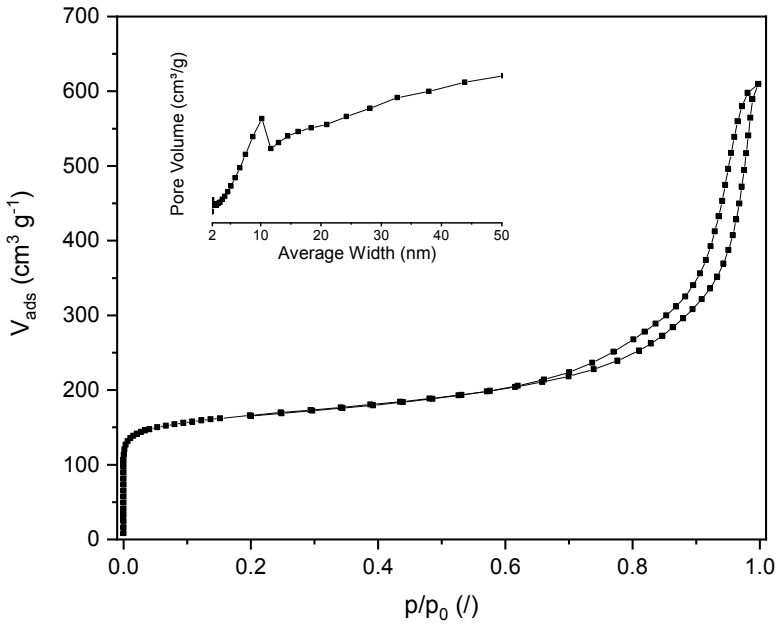

Fig. S6. N_2 physisorption of zeolite H-Beta, (inset) BJH distribution plot.

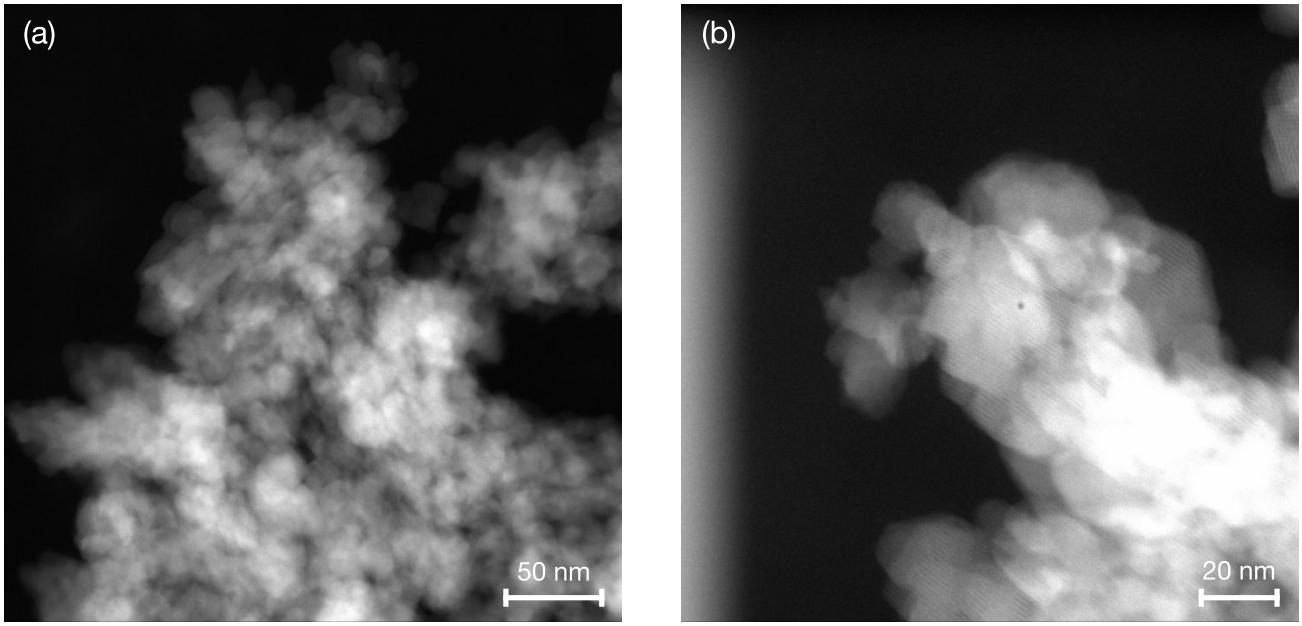

Fig. S7. STEM images of zeolite H-Beta.

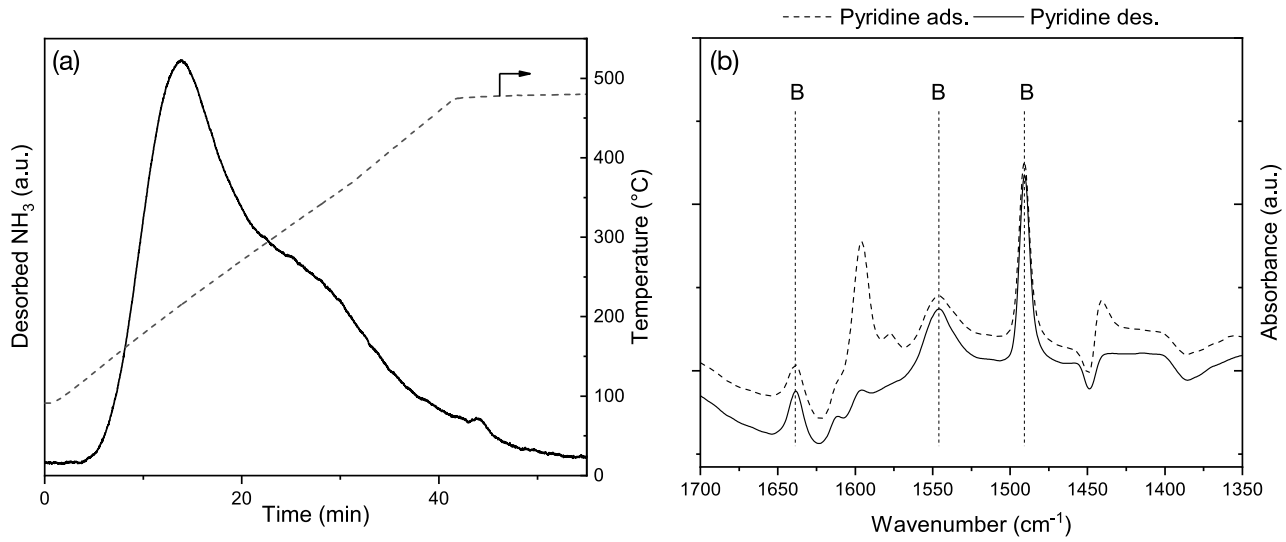

Fig. S8. Characterization of the acidity of zeolite H-Beta by (a) NH_3-TPD and (b) pyridine adsorption (dash line) and desorption (solid line) in cyclohexane by ATR-IR spectroscopy (B indicates vibrational bands associated with pyridine bonded to Brønsted acid site).

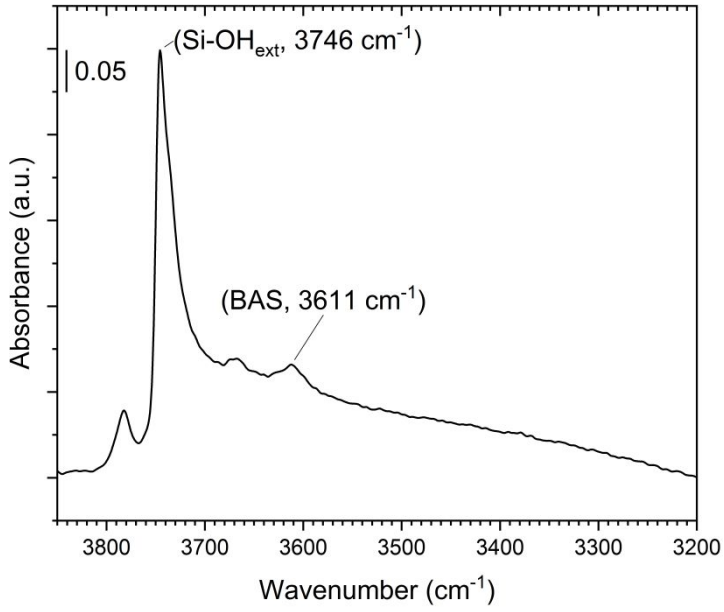

Fig. S9. Transmission IR spectrum of H-Beta after drying for 1 h at 500 °C with residual pressure below 10^{-3} mbar. BAS = 3611 cm^{-1}, Si-OH_{ext} = 3746 cm^{-1}.

4. Catalytic study

Table S1. Results of the kinetic model for the kinetic study with various water content in OME_1.

Run	H_2O wt % in OME_1	Temperature (°C)	RMSE[a]	$k_{OME,f}$ ($L \cdot mmol^{-1} \cdot min^{-1}$)
K1	0.03	25	0.56	1.421
K2	0.03	30	0.55	2.733
K3	0.03	35	0.59	4.917
K4	0.21	40	0.53	0.272
K5	0.21	50	0.54	1.065
K6	0.21	60	0.65	2.586
K7	0.44	50	0.45	0.114
K8	0.44	60	0.49	0.430
K9	0.44	70	0.53	1.013

[a] RMSE = Root Mean Square Error

The values of the apparent activation energy ($E_{a,app}$) and the frequency factor (A) for each water concentration were derived using the linearized Arrhenius equation (Table S2). The uncertainty in the apparent activation energy (σ_m) and the uncertainty in the frequency factor (σ_b) were calculated from data generated from the linearized Arrhenius equation, using the following formulae:

$$\sigma_m = m\sqrt{\frac{(1/R^2 - 1)}{n-2}} \qquad \text{Eq. (S1)}$$

$$\sigma_b = \sigma_m\sqrt{\frac{\sum x^2}{n}} \qquad \text{Eq. (S2)}$$

Table S2. Results from the linearized Arrhenius equation for various water contents in OME_1.

H_2O in OME_1 (wt. %)	$E_{a,app}$ (kJ/mol)	A (/)
0.027 ± 0.005	94.8 ± 0.3	$(5.9 \pm 0.2) \cdot 10^{13}$
0.238 ± 0.039	97.8 ± 1.2	$(5.7 \pm 0.8) \cdot 10^{12}$
0.436 ± 0.003	100.7 ± 1.3	$(2.3 \pm 0.3) \cdot 10^{12}$

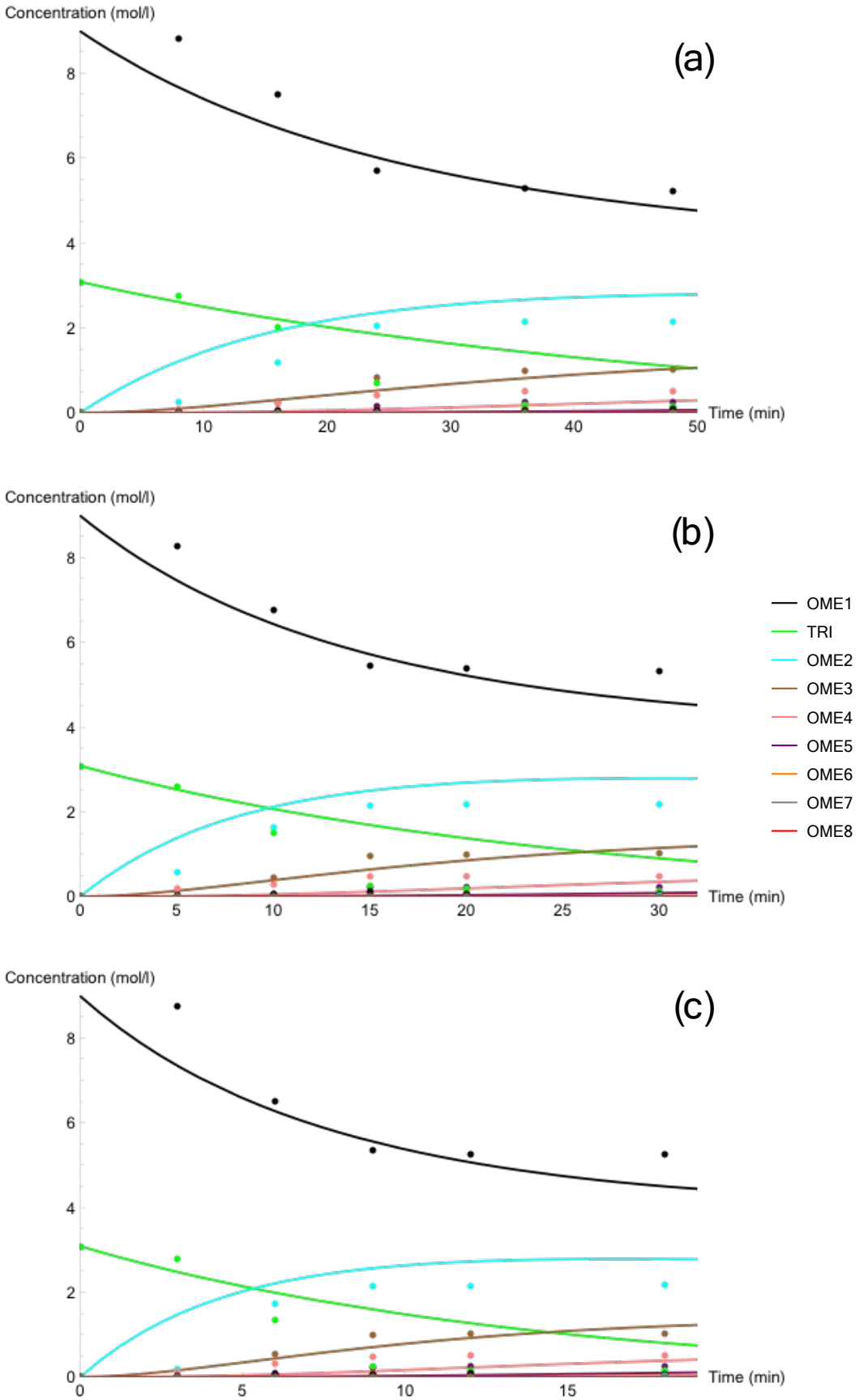

Fig. S10. Concentration of the various components vs. time (OME_1/TRI: 3.3; 0.5 wt % H-Beta) for experiments with OME_1-0.03-H_2O. (a) K1 at 25 °C, (b) K2 at 30 °C and (c) K3 at 35 °C. The model output is given by the solid lines.

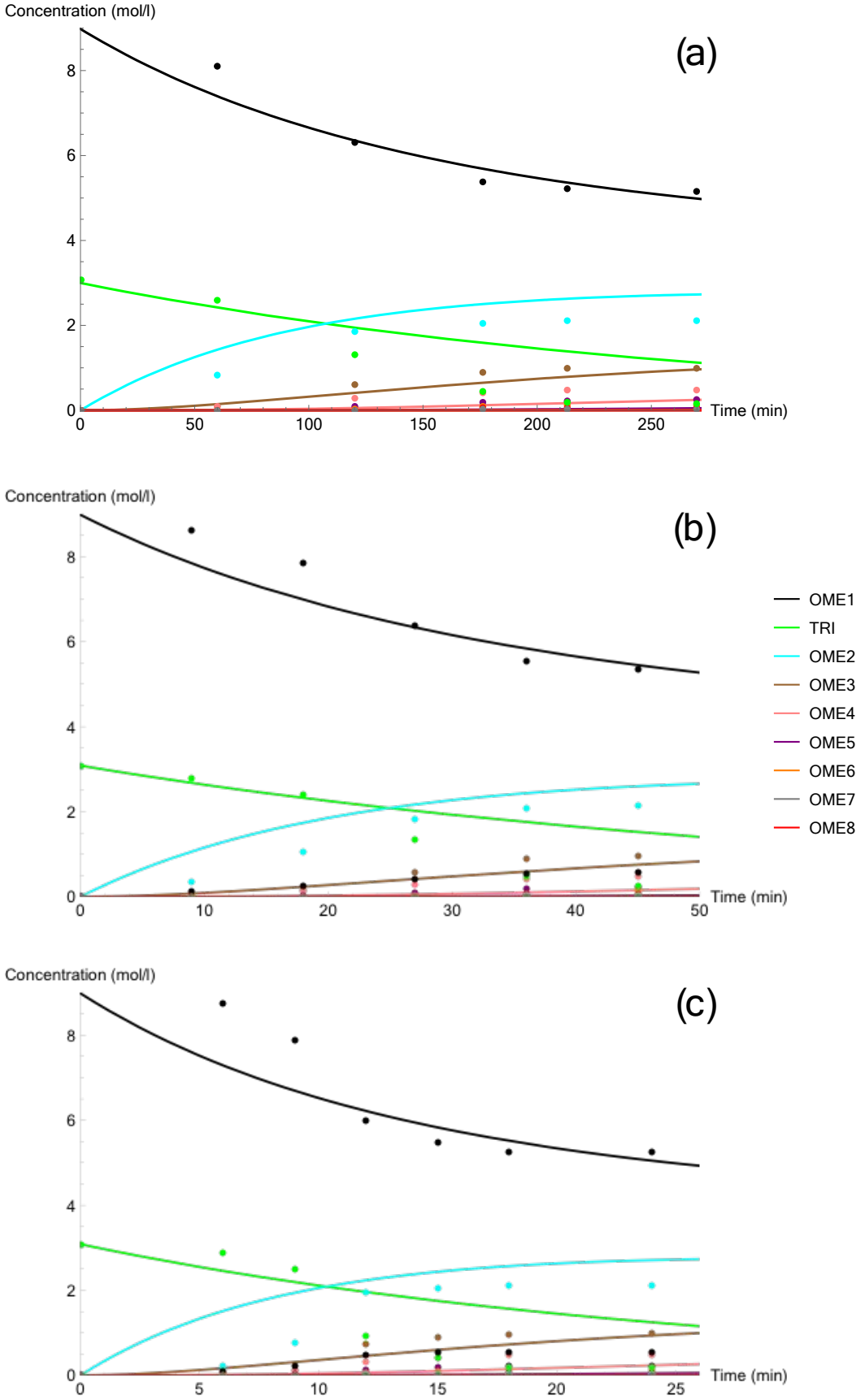

Fig. S11. Concentration of the various components vs. time (OME_1/TRI: 3.3; 0.5 wt % H-Beta) for experiments with OME_1-0.21-H_2O. (a) K4 at 40 °C, (b) K5 at 50 °C and (c) K6 at 60 °C. The model output is given by the solid lines.

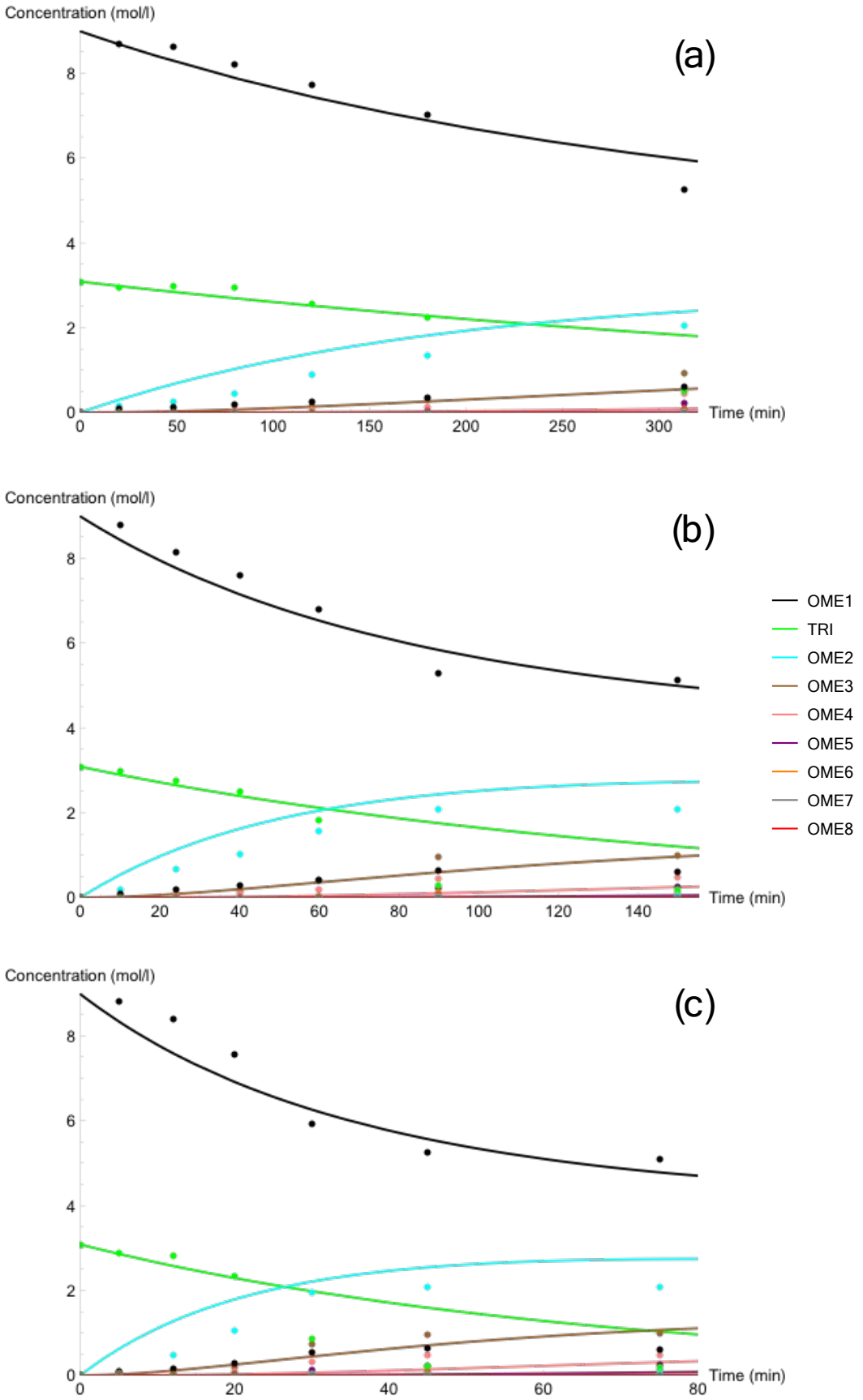

Fig. S12. Concentration of the various components vs. time (OME_1/TRI: 3.3; 0.5 wt % H-Beta) for experiments with OME_1-0.44-H_2O. (a) K7 at 50 °C, (b) K8 at 60 °C and (c) K9 at 70 °C. The model output is given by the solid lines.

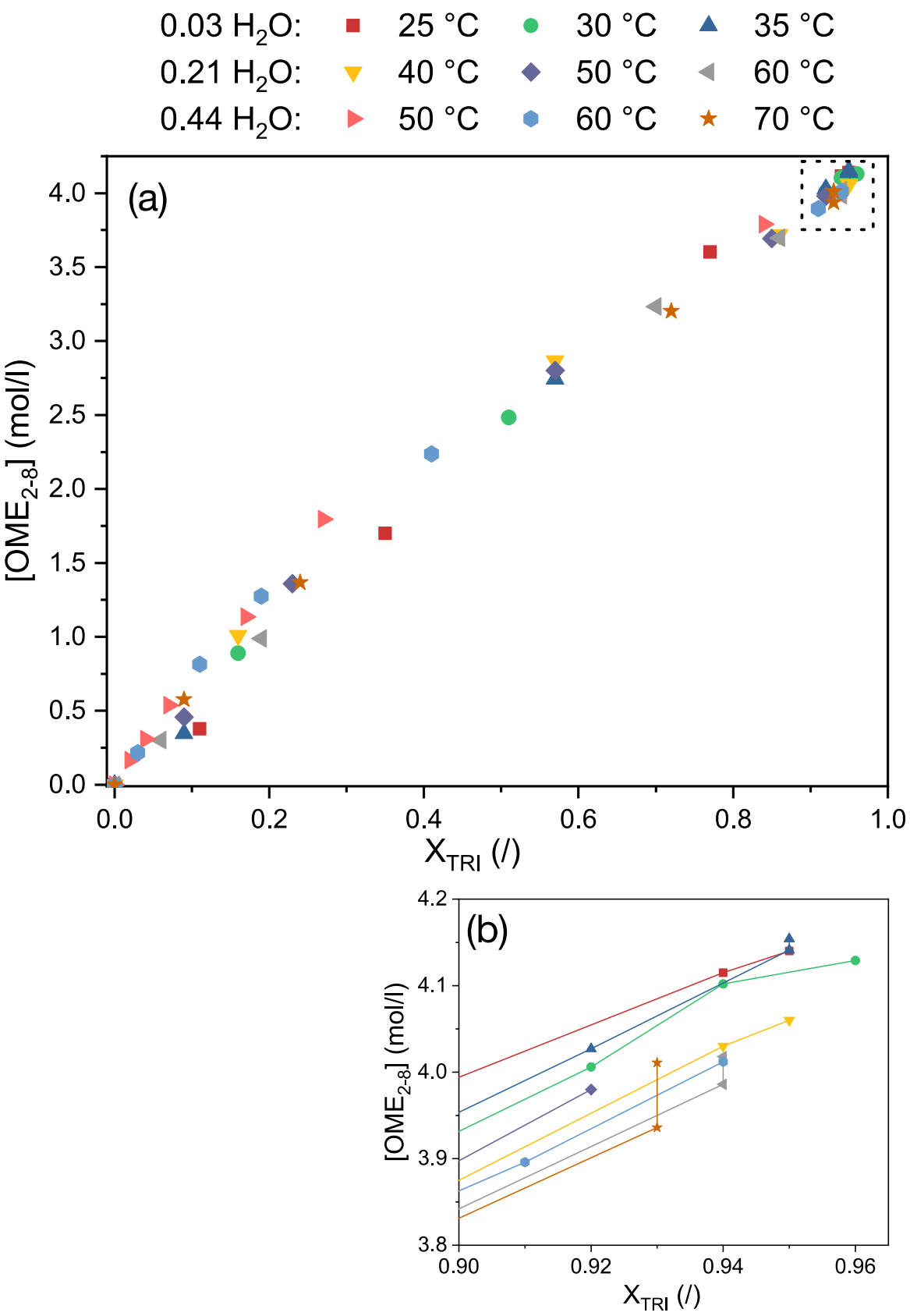

Fig. S13. (a) OME_{2-8} concentration vs. TRI conversion X_{TRI} for the synthesis of OME using various water concentrations in OME_1. (b) Magnification of the dashed square in (a).

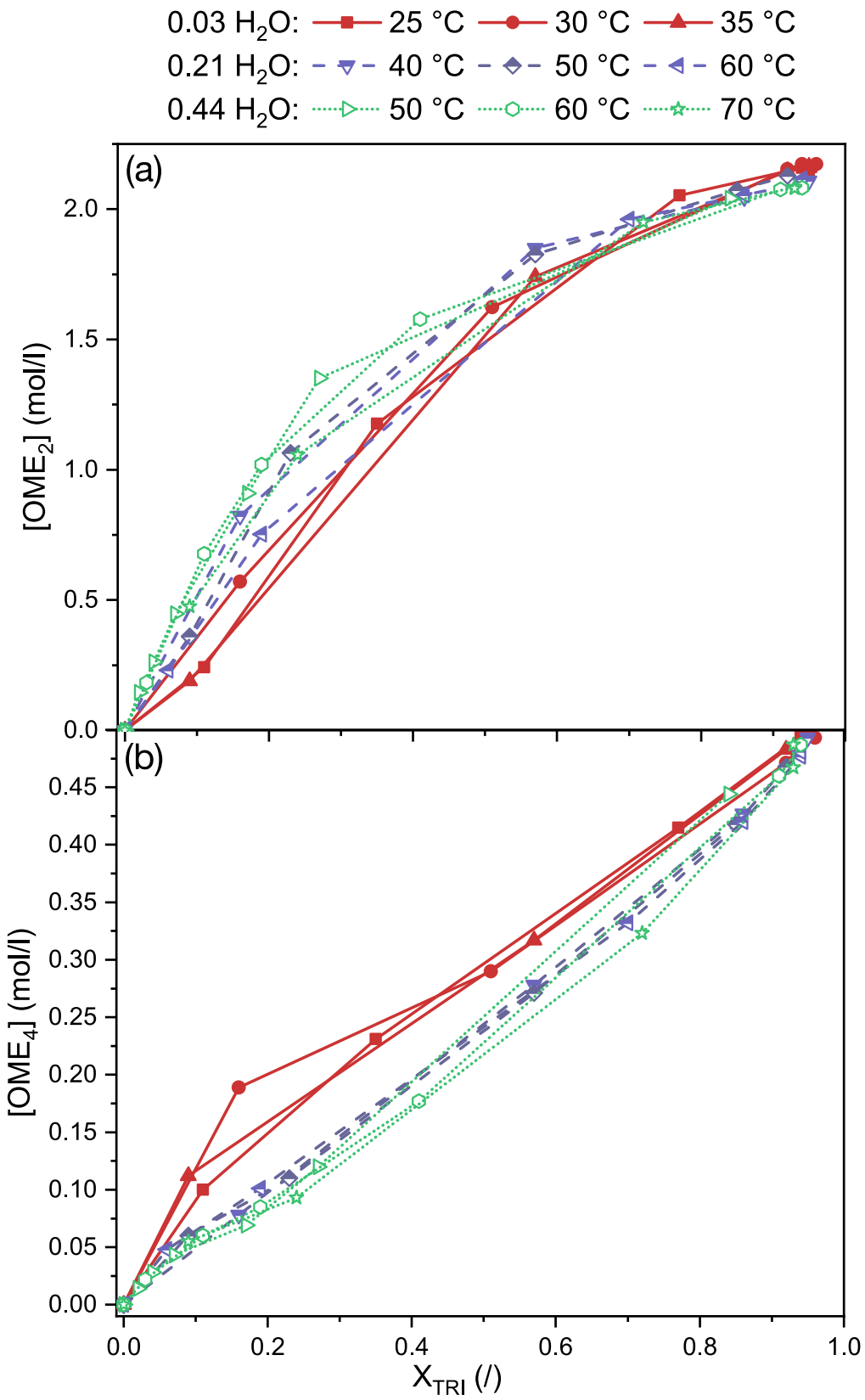

Fig. S14. (a) OME_2 concentration and (b) OME_4 concentration vs TRI conversion X_{TRI} for the synthesis of OME using various water concentrations in OME_1.

5. Modulation-excitation attenuated total reflectance infrared spectroscopy

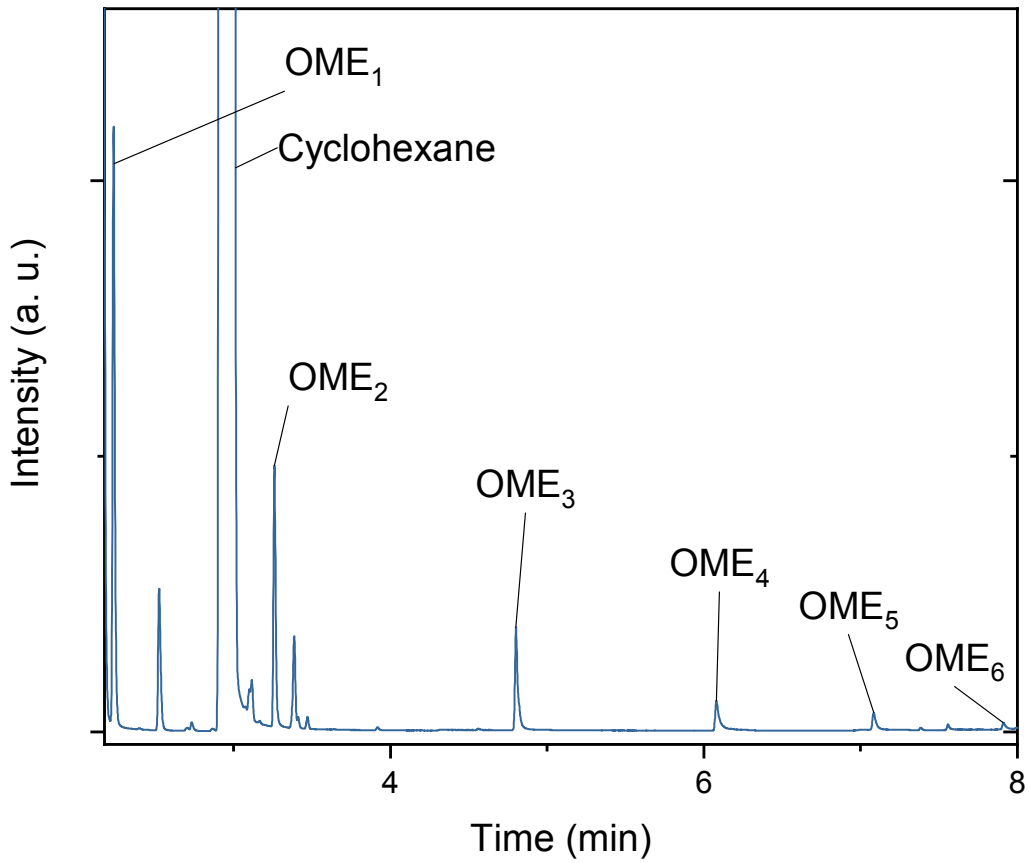

Fig. S15. Chromatogram after 5 min of reaction of 10 mM DMM and TRI in cyclohexane (10 wt % H-Beta and T = 25 °C).

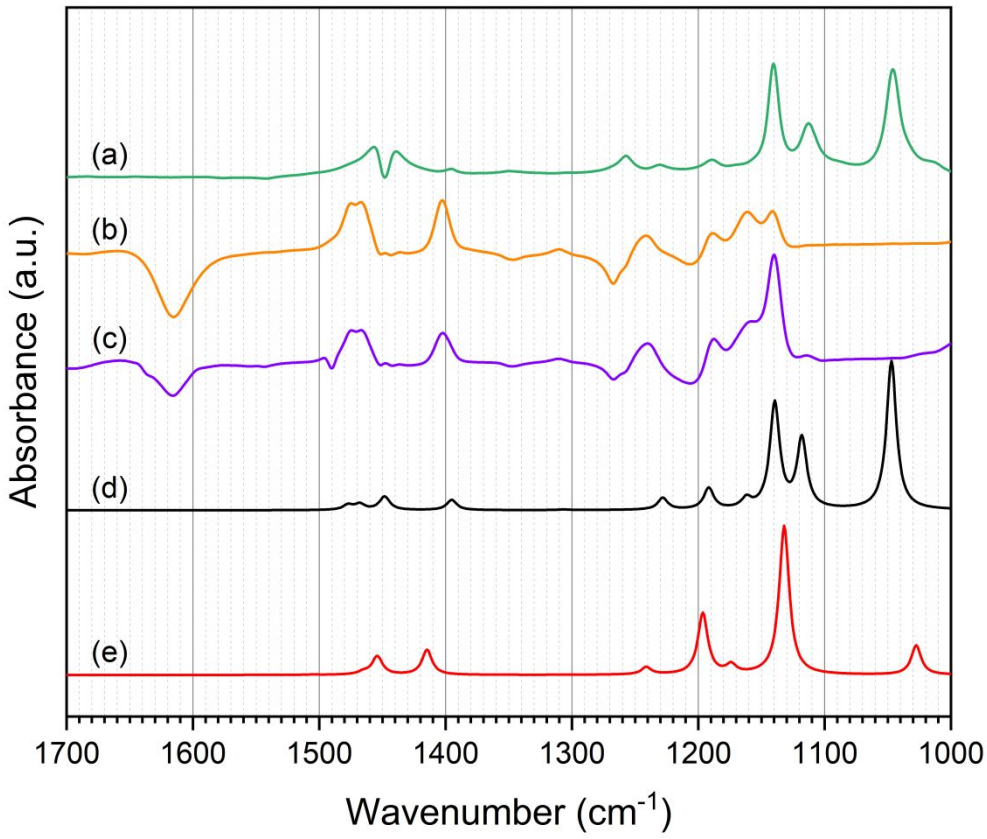

Fig. S16. (a) IR spectrum of OME_1 in cyclohexane (10 mM). Phase-resolved spectra (φ^{PSD} = 290°) obtained during adsorption-desorption of OME_1 (b) with and (c) without pyridine. Simulated vibrational spectra of (d) bent and (e) linear isomers of OME_1 in cyclohexane.

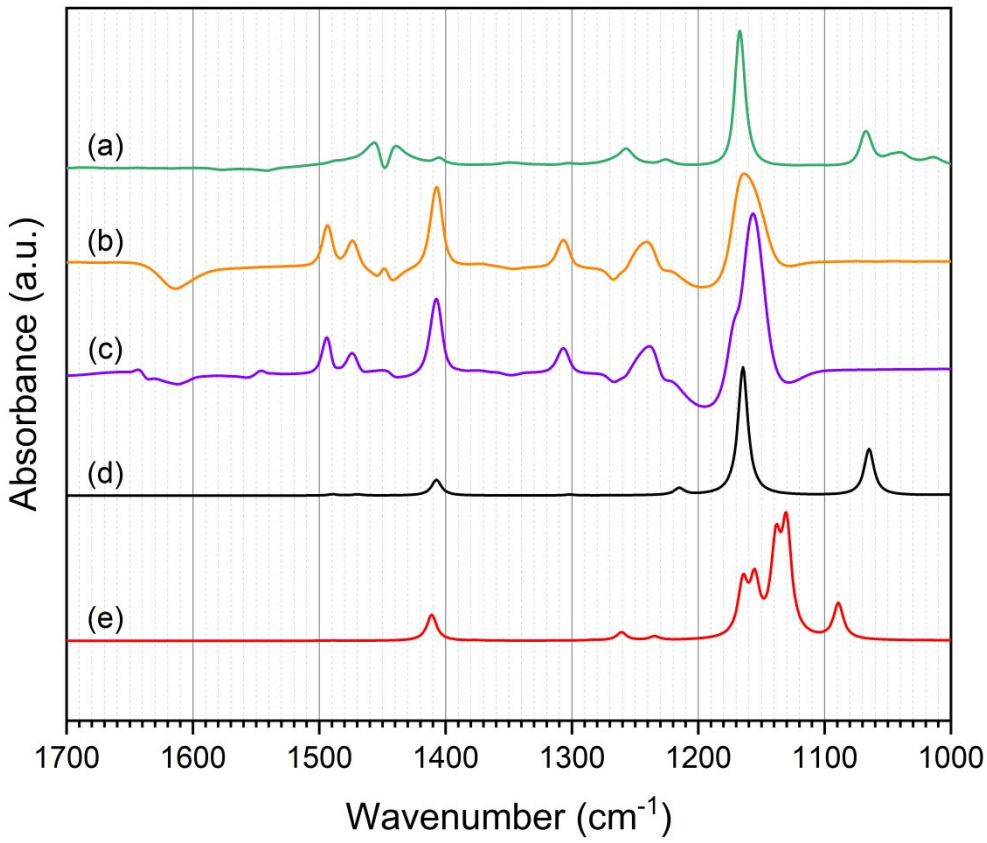

Fig. S17. (a) IR spectrum of TRI in cyclohexane (10 mM). Phase-resolved ATR-IR spectra (φ^{PSD} = 290°) obtained during adsorption-desorption of OME_1 (b) with and (c) without pyridine. Simulated vibrational spectra of (d) chair and (e) boat isomers of TRI in cyclohexane.

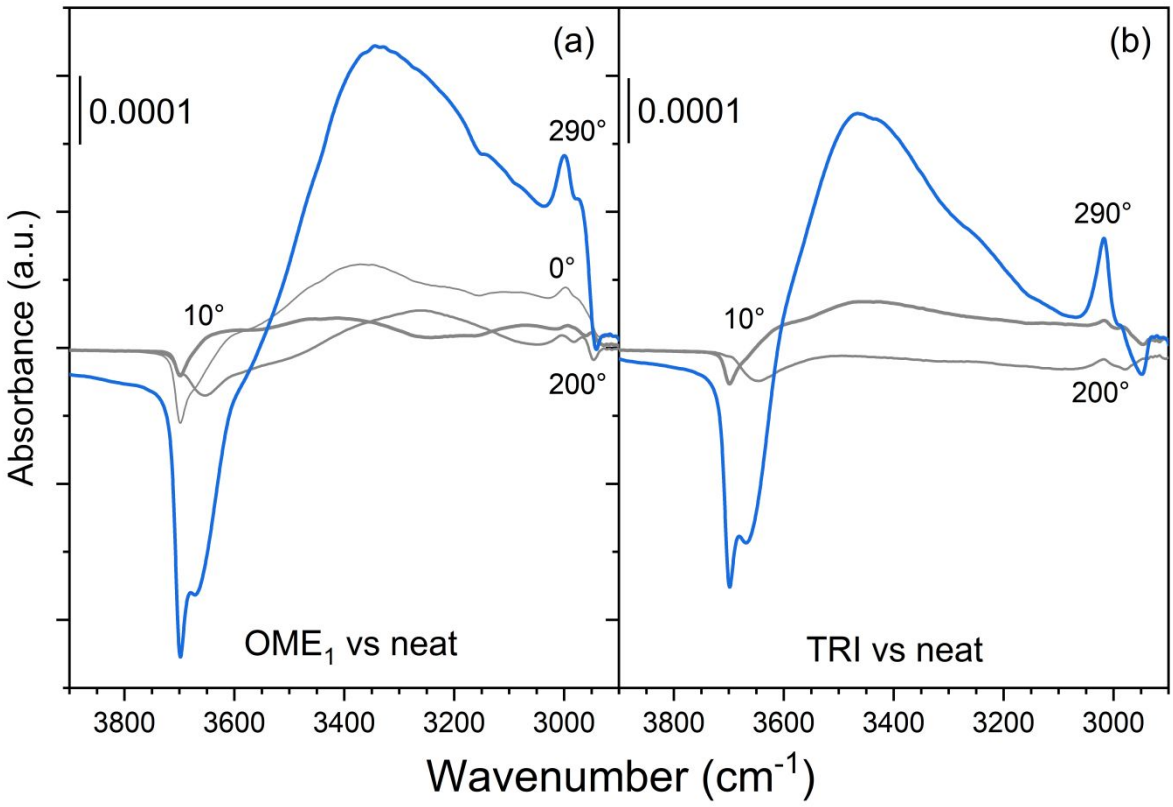

Fig. S18. Phase-resolved ATR-IR spectra during adsorption-desorption of (a) OME_1 and (b) TRI.

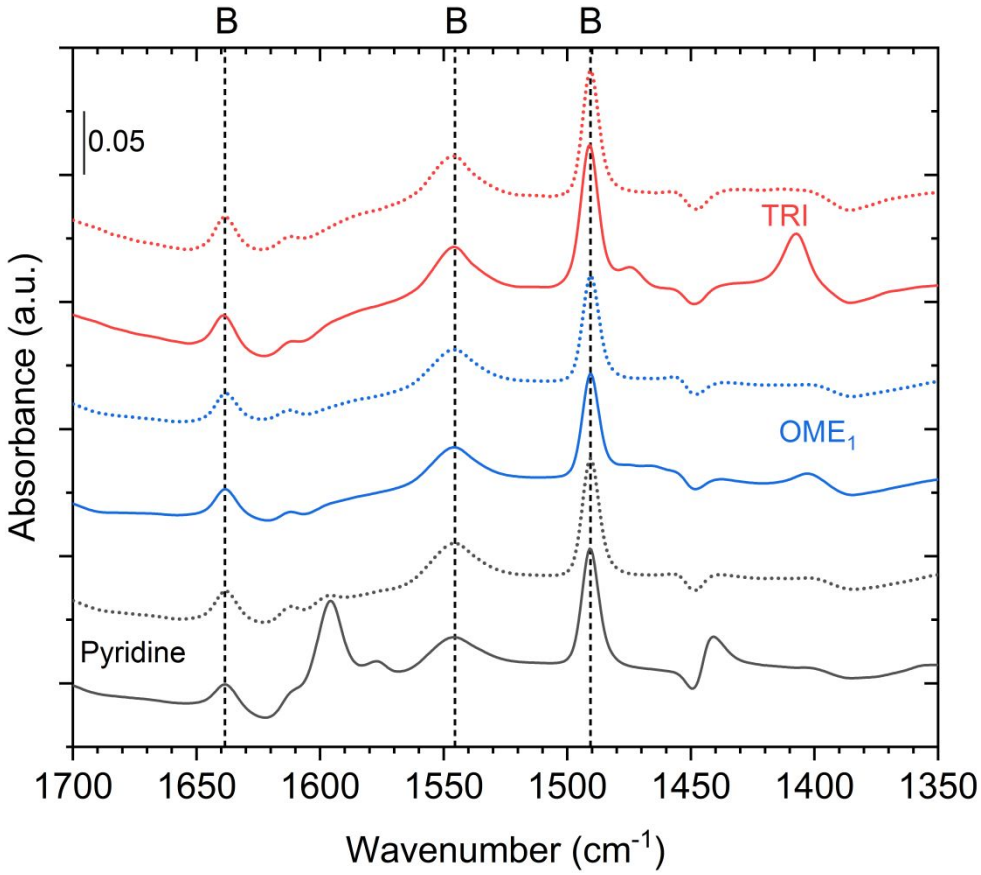

Fig. S19. ATR-IR spectra obtained during adsorption (plain line) and desorption (dashed line) of pyridine (black), followed by adsorption-desorption of OME_1 (blue) and TRI (red) on H-Beta in cyclohexane.

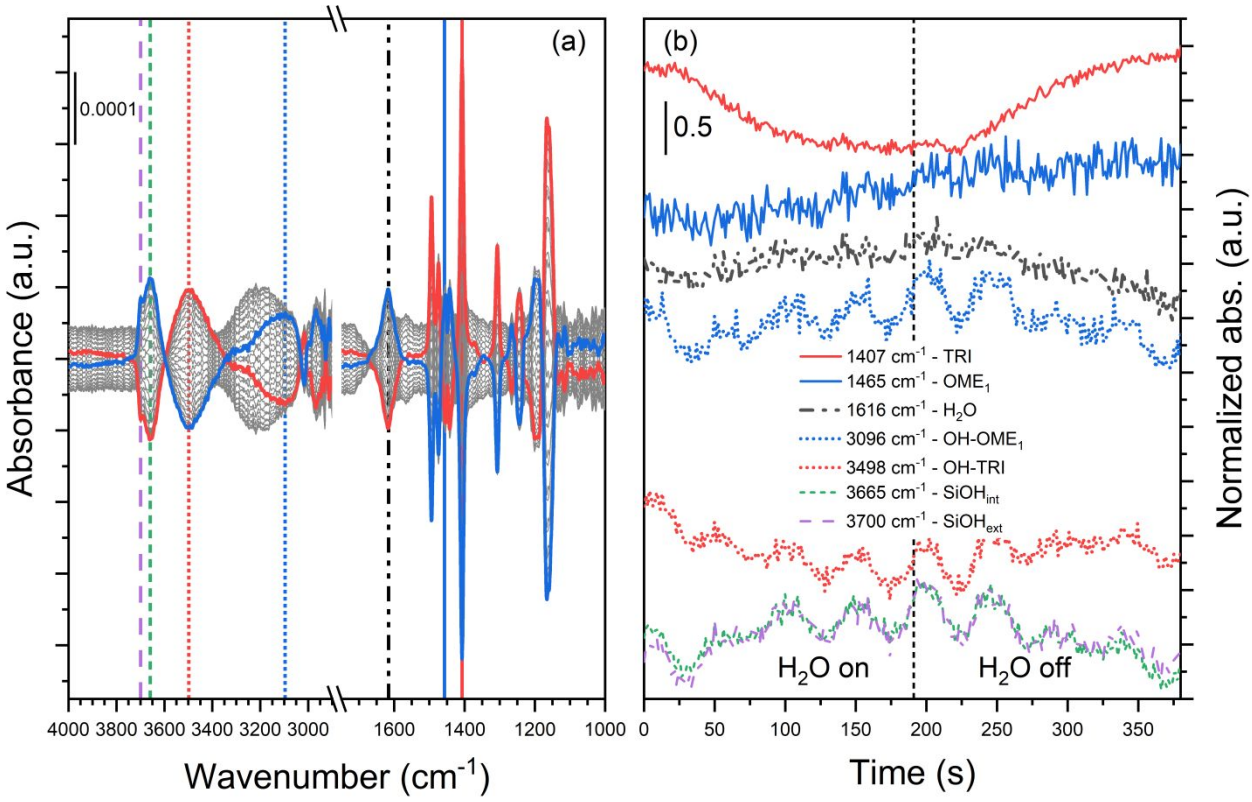

Fig. S20. Phase-resolved ATR-IR spectra and time-dependent traces of modulation experiments: OME_1 + TRI vs. OME_1 + TRI + H_2O. Vertical lines in (a) identify signals whose time-dependence is displayed in (b); the same line patterns and colors are used.